Highly charged ion densities and ion confinement properties in an electron-cyclotron-resonance ion source

G. Douysset,[1,*] H. Khodja,[1] A. Girard[1], and J. P. Briand[2]
[1]*Département de Recherche Fondamentale sur la Matière Condensée/SI2A, CEA Grenoble, 17 rue des Martyrs 38054 Grenoble Cedex, France*
[2]*LPAN, Université P.M. Curie, Case 74, 4, place Jussieu, 75275 Paris, France.*
(Received 16 April 1999)

Absolute ion densities in an electron-cyclotron-resonance ion source (ECRIS) plasma have been measured using high-resolution x-ray spectroscopy of $(n=2)\rightarrow(n=1)$ emission lines from highly charged argon ions. Ion densities have been correlated to extracted currents. The evolution of the ion confinement times with charge state has been investigated for various plasma parameters: a linear increase of the confinement time with charge was found. This result leads to a better understanding of the ion confinement mechanism in ECRIS plasmas.

PACS number(s): 52.50.Dg, 52.70.La, 29.25.Ni, 52.55.Jd

I. INTRODUCTION

Electron-cyclotron-resonance ion sources (ECRIS's) are devices designed for intense highly charged ion beam production. They are mirror machines where a plasma is heated by a high-frequency (hf) wave, usually between 10 and 18 GHz [1]. A resonant coupling between the wave and the electrons occurs when electrons cross a particular magnetic surface—the resonant surface—where the Larmor frequency is equal to the wave frequency. It leads to an increase of the perpendicular velocity (relatively to the magnetic flux lines). The heated electrons are trapped in a minimum-B structure. It has been shown that the resonance surface defines a volume where most of the particles are trapped [2]; its typical volume is about 25 cm^3 depending on magnetic field parameters.

Both theoretical [3] and experimental [4] works have shown that these plasmas are far from thermodynamical equilibrium. The electron distribution function (EDF) is strongly non-Maxwellian and can be schematically represented by three populations: a cold one, whose typical energy lies around the plasma potential ($\langle E_e\rangle \approx 50$ eV), a warm one, responsible for ionization processes, and a hot one well confined in the mirror. The typical range of electron density of these plasmas is between 10^{11} and $10^{12}\,cm^{-3}$ depending on ion source parameters [5]. As the time scale of the electron-ion collisional heating is much longer than the ion confinement times, the ionic energy is low [6]. Moreover, owing to a strong ion-ion collision rate [6], ions of any species and charge have the same temperature (around 1 eV [7]).

Many plasma parameters such as electron density [5], electron population temperatures [4], and ionic temperature [7] have been measured in various experiments with a relative good agreement with theoretical predictions. The measurement of highly charged ion density is also of great importance for understanding and upgrading ECRIS performances. This gives access to the confinement times of the ions, which are directly related to the ultimate performance of the ECRIS.

A previous experiment was made in the vacuum ultraviolet (vuv) range for low-charge nitrogen ion density measurement by Vinogradov *et al.* [8]. An attempt was also made in the x-ray range by Grübling *et al.* [9]. However, as a low-resolution spectrometer was used, and a Maxwellian EDF was supposed, the accuracy of the results was limited. A comparable study, but for medium-charge-state ions (up to O^{5+}), in the vuv range, has also been performed in the Constance B device [10].

In this paper, we describe an experiment carried out on an ECRIS operated with argon. Quasisimultaneous measurements of x-ray $K\alpha$ emission and bremsstrahlung were performed and led to the determination of the EDF and the ion charge state distribution (CSD) in the plasma. At the same time the source was biased to a positive voltage (+20 kV) in order to extract ions. Current spectra were recorded and compared to ionic densities. Correlations between the CSD in the extracted beam and that in the plasma have been investigated.

II. EXPERIMENT

Spectroscopic measurements were performed on the plasma of the so-called Caprice 10 GHz ECRIS, similar to that described in [11]. The source was operated under various plasma conditions with argon, possibly adding oxygen to enhance high-charge-state currents using the well-known gas mixing technique [12,13].

Extracted ions were analyzed in mass and charge by a dipole magnet and currents were measured by a polarized Faraday cup. The highest detectable charge state was Ar^{16+} (typical current 0.6 μA). Stability of the plasma parameters for a range of several hours was achieved using a self-regulated gas injection system.

Preliminary experiments were carried out with a low-resolution nitrogen-cooled high-purity germanium (HPGe) type of detector and showed that the $K\alpha$ line shifts and

*Present address: Department of Atomic Physics, Stockholm University, Frescativägen 24, 10405 Stockholm, Sweden.

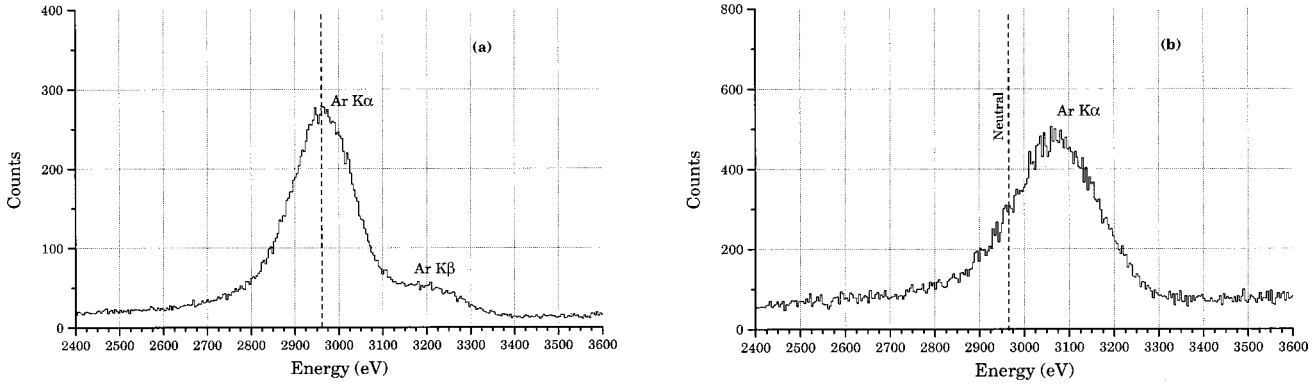

FIG. 1. Low-resolution $K\alpha$ emission spectra of argon, acquisition time 700.0 s. (a) 20 W, (b) 900 W.

broadens as more highly charged ions are extracted from the source. At the same time the $K\beta$ line disappears indicating the removal of all M electrons ($q>8+$) (Fig. 1). Although the resolution of the detector (typically 150 eV at 3 keV) is insufficient to separate each individual line, this indicates an increase of the mean charge state of the plasma.

As the energy shift of argon $K\alpha$ is only about 20 eV for each L electron removed ($8+<q<16+$) [14], we designed and built a high-resolution Bragg type spectrometer. For that purpose, we used bent Ge(111) and Si(111) crystals in Johann geometry [15]. The radii of curvature were 1000 mm. Crystal dimensions were 80 mm$\times$8 mm; however the lighted area was limited to 30 mm$\times$8 mm by lead slits in order to reduce aberrations. Dispersive crystals were mounted under vacuum on a rotating and translating plate. Crystals were set up 2200 mm away from the plasma center on the ECRIS main axis.

A linear position-sensitive proportional counter [16] located on the Rowland circle was mounted on a movable arm. The filling gas was a mixture of xenon and 15 mol % of C_2H_6 ($P=1.5$ bar). The entrance window was made of thin Kapton (18.75 μm). As the detection depth is close to 8 mm the absolute efficiency at 3 keV was found to be 75% on the 70-mm detection length. Spatial resolution was found to be 200 μm at 6.4 keV.

In order to determine the absolute ionic densities, the absolute efficiency of the spectrometer has been carefully studied. Solid angle and emitting volume have been computed by simulating photon paths through the spectrometer. Theoretical Bragg diffraction patterns were taken from the XOP code [17]. The observable energy range for a fixed crystal orientation was also computed ($\approx$ 70 eV) and was found to match the experimental data. The energy resolution was 3.1 or 2.1 eV at 3140 eV ($\lambda/\delta\lambda\approx 1000-1500$) depending on the analyzing crystal.

Between the ECR plasma and the crystal chamber an online micro x-ray tube was designed and mounted for energy calibration purpose.

The crystal was also made extractable to record the axial photonic emission with the low-resolution HPGe detector. In this case a movable collimation system could be used.

An overview of the experiment is given in Fig. 2.

The absolute efficiency of the low-resolution detector was computed by a Monte Carlo simulation and is presented in Fig. 3. This result was successfully checked by comparison of the spectra recorded simultaneously with a well-known Si(Li) detector. Solid angle and emitting volume were also precisely computed.

III. PHOTON EMISSION FROM ECR PLASMAS IN THE X-RAY RANGE AND DATA PROCESSING

A. Bremsstrahlung emission

Electron interactions with the residual gas and the ions inside the plasma chamber lead to bremsstrahlung emission which is characteristic of the EDF. This is a powerful diagnostic for the warm and the hot electron population study [4,18].

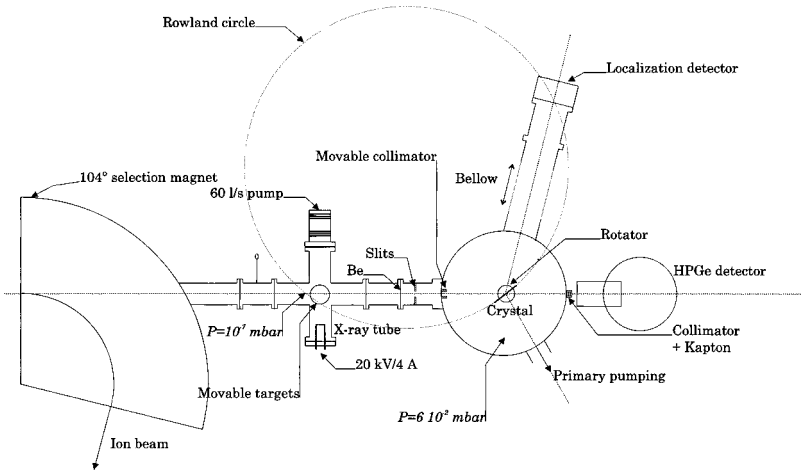

FIG. 2. Overview of the x-ray diagnostics mounted on the Caprice 10-GHz ion source.

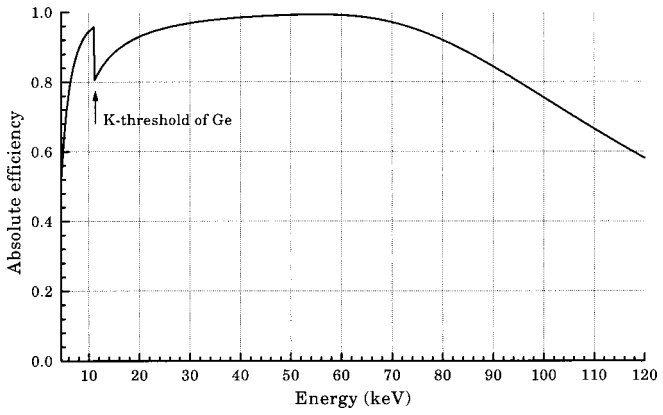

FIG. 3. Computed absolute efficiency of the low-resolution spectrometer.

The emissivity under an observation angle $\Omega(\theta)$ from a multispecies plasma can be written as

$$J(h\nu)=(h\nu)N(h\nu)=\sum_{q=\text{neutrals}}^{q_{\max}} n_q(h\nu)\int_{h\nu}^{\infty}\frac{d^2\sigma_q(E_e,h\nu,\theta)}{d\Omega(\theta)d(h\nu)}\times f(E_e)\beta(E_e)c\,dE_e, \quad (1)$$

where $d^2\sigma_q(E_e,h\nu,\theta)/d\Omega(\theta)d(h\nu)$ is the double differential bremsstrahlung cross section, $f(E_e)$ is the relativistic EDF, n_q is the density of charge state q, $\beta(E_e)c$ is the velocity associated with an electron of energy E_e, and $N(h\nu)$ is the number of photons emitted per second and per unit of photon energy $h\nu$. The sum is performed over all the charge states present in the plasma. As the energy emitted during bremsstrahlung reaction increases according to Z^2, where Z is the atomic number of the target, *e-e* emission was neglected in Eq. (1). Even though no theoretical data can be found for the dependency of double differential cross section on charge state, the estimation of the single differential cross section $d\sigma_q(E_e,h\nu)/d(h\nu)$ variation with ion charge [19] shows that in our case, no significant correlation with ion charge can be found. The reason is that we used low-Z gas (oxygen or argon) and we started the EDF determination above the *K*-shell excitation threshold of argon ions (typically 3 keV). Therefore, we used an interpolation of bremsstrahlung cross sections for neutrals from the work of Kissel [20]. Consequently, one can get access to an approached EDF by fitting the experimental emissivity spectrum with the one produced by two Maxwellian functions. However, the total target density (sum of neutral and total ionic densities) has to be fixed. Reasonable values are in the range of 10^{11} cm^{-3}. This value can be checked *a posteriori*.

B. Discrete line emission

X-ray line emission from ECR plasmas is related to various collisions: electronic inner-shell ionization and excitation, dielectronic recombination, charge exchange reactions, or radiative recombination.

As EDF's are always very energetic, the dielectronic recombination rates, taken from [21], are low compared to the dominant processes, which are inner-shell ionization and *K-L* excitation.

Charge exchange and radiative recombination reactions lead to $K\alpha$ emission only after collisions on Ar^{17+} or Ar^{18+}.

We have used the cross sections for inner-shell ionization computed by Golden and Sampson [22] that model the shape for successive charge states. A statistical weight was used to populate all the possible initial states $|n'L'S'\rangle$. Excitation cross sections of Ar^{17+}, Ar^{16+}, and Ar^{15+} are taken from [23–25] and for $8+<q<15+$ excitation rates were interpolated.

The energy and fluorescence yields for each transition $|n'L'S'\rangle\rightarrow|nLS\rangle$ have been taken from multiconfiguration Dirac-Fock (MCDF) calculations of Indelicato [26,27] and Chen [28–31].

IV. EXPERIMENTAL SPECTRA

A. $K\alpha$ spectra and extracted ion currents

Several spectra were recorded for various plasma conditions from low to high hf injected power. They are presented in Fig. 4 together with extracted currents. The high-resolution spectrometer allowed us to separate clearly each individual $K\alpha$ line from ions of charge state above $9+$. Line identification was performed after energy calibration using MCDF calculations. An example of comparison between theoretical and experimental spectrum is given in Fig. 5. This confirms the statistical population of the initial states.

Several results appeared from the high-resolution spectra. First, a strong evolution connected with the injected power should be noticed. Moreover, it was always impossible to detect an ion in the plasma if it did not appear in the extracted current spectrum. The third result is that most of the ions are in their ground configuration before the *K*-shell excitation. Indeed, no line of doubly excited configurations such as $(1s2s2p^n)-(1s^22s2p^{n-1})$ $(n>1)$ could be detected. Then we may notice that the argon ionization rates are very close to 100% even for low hf injected powers $(P_{\text{hf}}\geqslant 150\,\text{W})$.

On the other hand, whatever the plasma parameters, it remained impossible to detect $K\alpha$ lines of H-like argon. This indicates that the Ar^{17+} density in the plasma is always very small.

B. Bremsstrahlung spectra

After the $K\alpha$ spectra recording, the bremsstrahlung emission was measured by the HPGe detector keeping all the plasma parameters constant. The emissivity measurements started from 4.5 keV to avoid contamination of the spectra by argon $K\alpha$ lines. EDF's were then extrapolated to the *K*-excitation threshold (3.3 keV).

No $K\alpha$ line from wall or electrode materials (Fe, Cu, Co) was detected, which confirmed the efficiency of the collimation system.

Experimental and simulated emissivities of two typical plasmas are presented in Fig. 6. The high-energy contribution increases for high-performances plasmas (from 48 keV at 150 W to 60 keV at 500 W), whereas the lower energy is kept nearly constant (9.5 keV at 150 W and 10 keV at 500 W). Numerical simulations by Perret [32] predicted that the

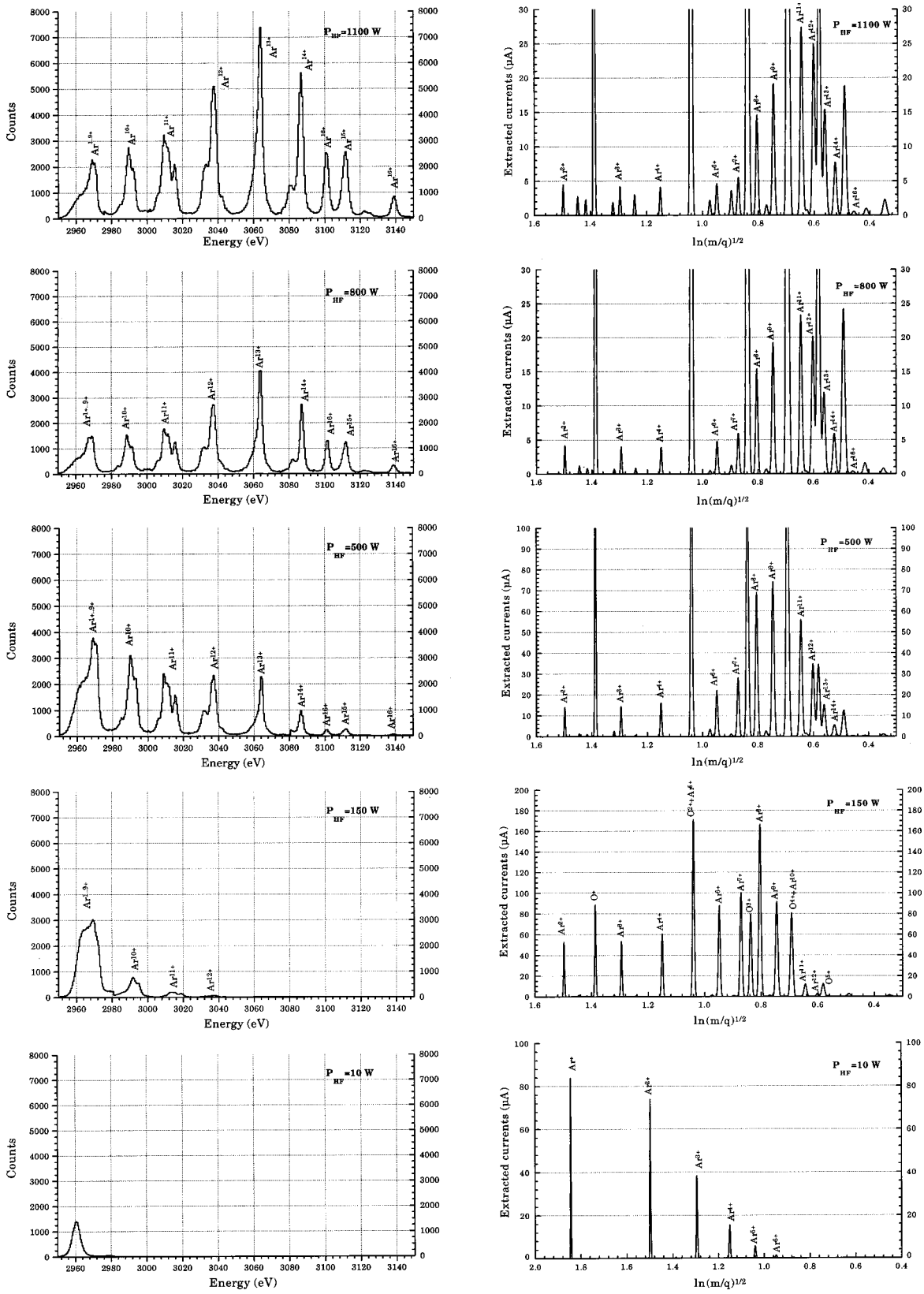

FIG. 4. High-resolution $K\alpha$ emission spectra of argon [Ge(111)] (acquisition time 100.0 s, hf powers 1100, 800, 500, 150, and 10 W) and the corresponding extracted current spectra (unlabeled peaks are from oxygen ions and impurities).

fraction of electrons of energy higher than a few keV is in the range of 20% to 50%. In our case, we check that the integral $\int_{\text{Thresh}}^{\infty} f(E)dE$ is $1.9\times10^{11}\,\text{cm}^{-3}$ at 150 W (Fig. 6) and $2.8\times10^{11}\,\text{cm}^{-3}$ at 500 W (same figure). The highest value obtained during the experiments was $5.7\times10^{11}\,\text{cm}^{-3}$, obtained at 1100 W for the optimum performance of the source for Ar^{16+}. These values are consistent with expected densities.

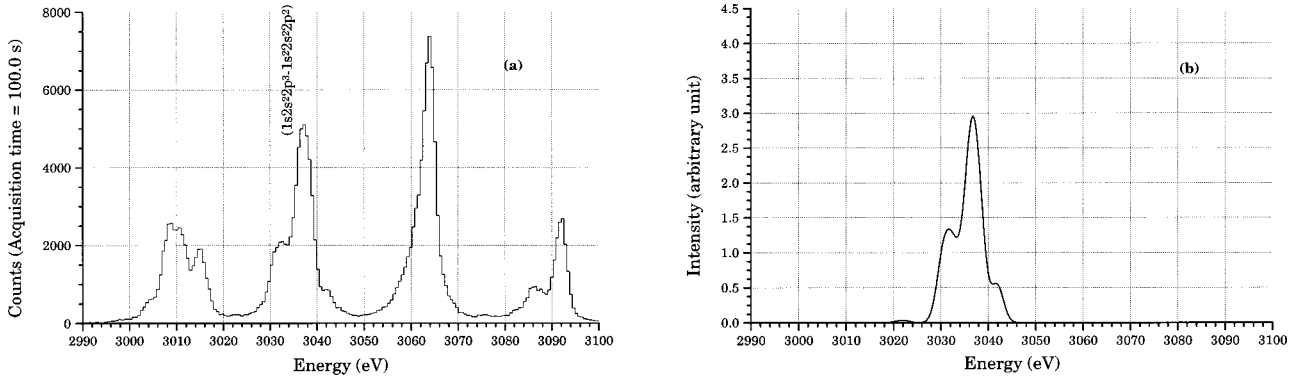

FIG. 5. Comparison between experimental (a) and theoretical (b) ($1s2s^22p^3$) deexcitation spectra (Gaussian profiles and statistical population are assumed).

V. RESULTS AND DISCUSSION

A. Ionic density measurements

Ion densities were deduced from x-ray spectra and EDF's using a steady state model (corona equilibrium). Writing the excited state production rate and recalling that the dominant processes are inner-shell ionization and *K*-*L* excitation, we get

$$\frac{dn_q^i}{dt} = n_e n_q^0 \langle \sigma_{\text{exc}}^{q\to q} v \rangle + n_e n_{q-1}^0 \langle \sigma_{\text{ion}\,K}^{(q-1)\to q} v \rangle - \frac{n_q^i}{\tau_i} = 0. \tag{2}$$

Here, n_e is the electron density, n_q^0 is the density of Ar^{q+} in the ground state, n_q^i is the density of Ar^{q+} in the excited state i, $\sigma_{exc}^{q\to q}$ and $\sigma_{\text{ion}\,K}^{(q-1)\to q}$ are core excitation and *K*-shell ionization cross sections to the excited level i, and τ_i is the total lifetime (radiative+Auger) of the excited state i. The Ar^{q+} $K\alpha$ line intensity is proportional to n_q^i/τ_i.

As the H-like argon density is negligible, and as most of the ions are in the ground configuration, the $^1P_1(1s2p)$ state of Ar^{16+} is populated only by excitation of He-like argon.

On the other hand, the density of Ar^{15+} can be deduced in two different ways: (i) the forbidden line $^3S_1(1s2s)-{}^1S_0(1s^2)$ is produced by inner-shell ionization of Ar^{15+} in the ground state; (ii) the lines $^2P_{3/2}(1s2s2p)-{}^2S_{1/2}(1s^22s)$ and $^2P_{1/2}(1s2s2p)-{}^2S_{1/2}(1s^22s)$ are produced by *K*-*L* excitation of Ar^{15+} in the $(1s^22s)$ configuration. These two determinations were found to be in excellent agreement.

Densities of other charge states were deduced by solving the system of coupled equations (2).

The ionic densities for three different ion source settings are presented in Fig. 7 together with the extracted currents. A very strong correlation appears: whatever the plasma parameters the extracted ion spectrum is an image of the densities in the plasma. This leads to important conclusions concerning the ion confinement times.

B. Ion confinement times

Ion confinement times τ_q were estimated using the following equation:

$$\tau_q = \kappa \frac{(2L)S}{2} \frac{n_q q e}{I_q}. \tag{3}$$

Here n_q is the density of Ar^{q+}, e is the charge of the electron, I_q is the measured electrical current of Ar^{q+}, $2L$ is the length of the plasma, and S is the area of the extraction hole; κ is the transmission efficiency of the beam line. Equal currents out of the two ends of the field lines of the mirror are assumed, which explains the factor of 2 in the denominator. This assumption is reasonable as the Caprice source works with a quasisymmetric mirror. From the derived densities

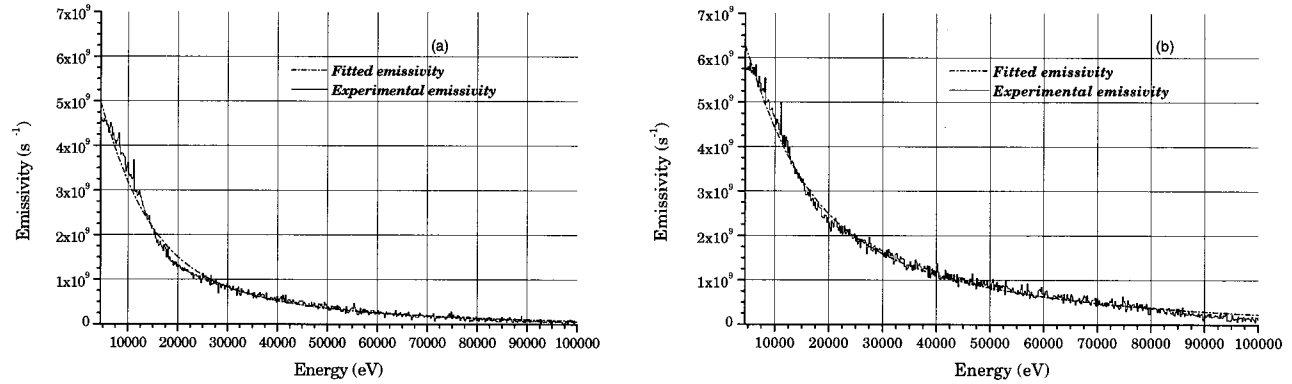

FIG. 6. Experimental and fitted (with two Maxwellians) emissivity curves of argon plasmas. (a) 150 W; colder temperature $T_c = 9.5$ keV, hotter temperature $T_h = 48$ keV and (b) 500 W; $T_c = 10$ keV, $T_h = 60$ keV.

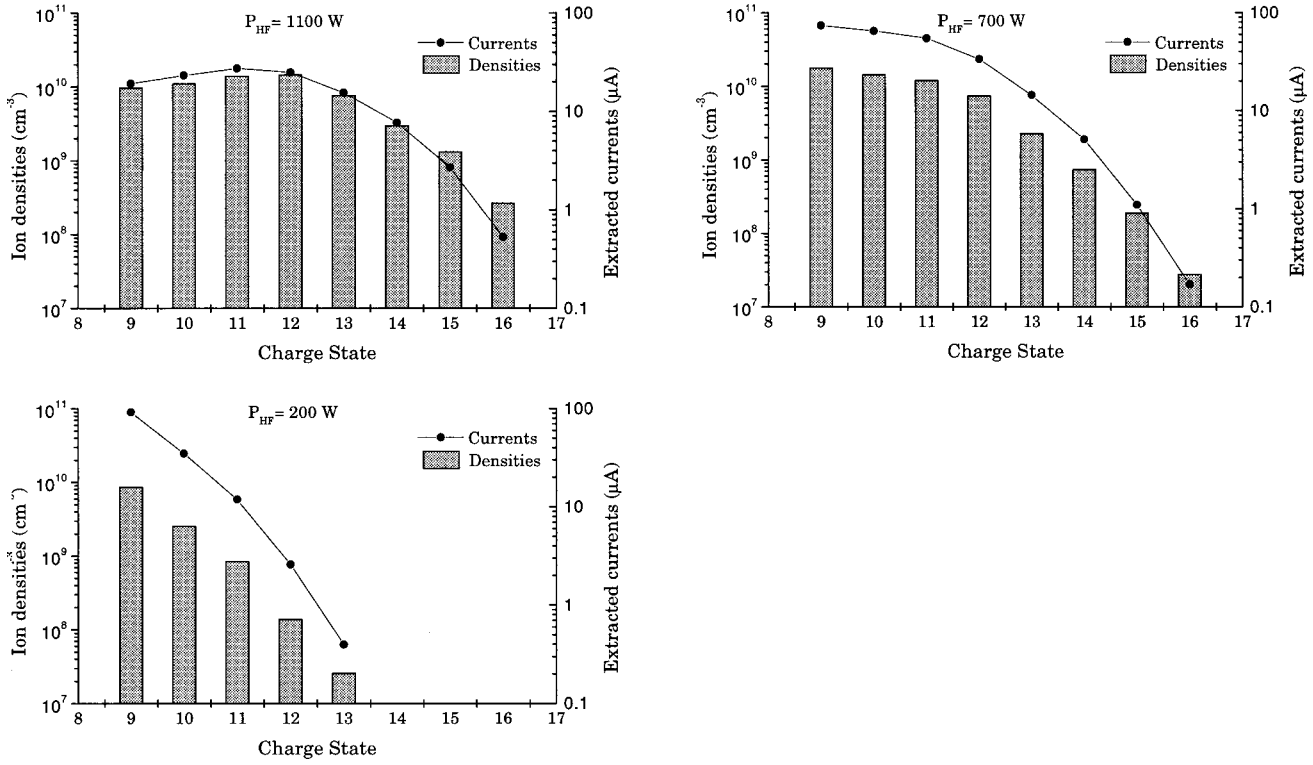

FIG. 7. Compared evolution of ion densities and extracted currents with charge state. Three typical plasmas are investigated from high to low injected hf power.

and measured currents it is therefore possible to have an estimate of the confinement times. The uncertainties related to the derived values have already been mentioned. Statistical errors are small, but systematic errors are difficult to estimate exactly: there is some slight uncertainty concerning the density of targets (see above) and also concerning the solid angle and the absolute calibration of the spectrometer; there is also some uncertainty related to the transmission of the beam line (75% transmission is assumed). From all these uncertainties it is most probable that the determination of the confinement times is reliable within a factor of 2.

Figure 8 shows the confinement times of Ar^{q+} ions for two plasmas: (a) at high (1100 W) hf power (left)—this plasma corresponds to the optimization of Ar^{16+} ($0.53\,e\,\mu$A)—and (b) at intermediate power (700 W), where the largest current for Ar^{12+} is obtained (right). The order of magnitude of the confinement times obtained is between 0.74 and 3.5 ms. This is consistent with recent results obtained for electron confinement times [33]. It is interesting to notice that the confinement time increases as the charge increases. This tendency is particularly clear in Fig. 8(a), where the confinement time varies between 1.5 and 3.5 ms for Ar ions beyond charge 9: to optimize high-charge states (here Ar^{16+}) it is necessary to maximize the confinement time. On the other hand, when only intermediate (Ar^{12+}) charges are to be optimized, the confinement time does not need to reach such high values [Fig. 8(b), 700 W]: it varies between 0.7 and 1 ms. Moreover, the slopes of the two lines [Figs. 8(a) and 8(b)] are different. In order to check this evolution the Ar^{17+} confinement time can be extrapolated. As the EDF is measured, the Ar^{17+} density and extracted current can be estimated. We found that this density is about 70 times smaller than that one of He-like argon. The estimated corresponding current is in the range of 7 nA. This

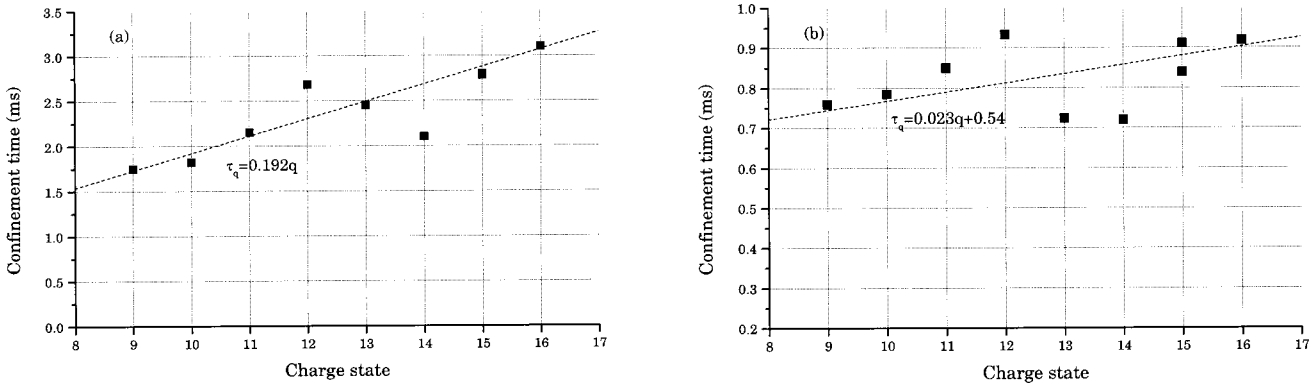

FIG. 8. Estimation of ion confinement times. (a) 1100 W (Ar^{16+} optimization); (b) 700 W (Ar^{12+} optimization).

confirms that the $K\alpha$ lines of Ar^{17+} are too weak to be detected by our spectrometer. In the same way one can get access to an approached value of the densities of $Ar^{q<9+}$. Then the unresolved $K\alpha$ line of $Ar^{q<10+}$ intensity can be roughly estimated. It appears that this value only slightly exceeds the experimental intensity.

C. Discussion

Several theoretical models of ion confinement in mirror plasmas have been proposed [34–36]. It was suggested that ions are trapped in a potential dip [37,2,38,39]. This negative potential $\Delta\phi$ would be produced in the center of the machine by high-energy electrons that are magnetically well confined. The resulting formula for ion confinement time in this case is [35]

$$\tau_q = R\frac{\sqrt{\pi}L}{v_{T_i}}\exp\left(\frac{|qe\,\Delta\phi|}{kT_i}\right). \tag{4}$$

Here R is the mirror ratio of the magnetic trap ($=B_{\max}/B_{\min}$), $2L$ is again the plasma length, v_{T_i} is the ion thermal velocity, and T_i is the ion temperature. So even for a low $\Delta\phi$ (lower than 1 V) the confinement time evolution with charge state could be very strong. However, this formula becomes highly questionable at high density, when the ions become very collisional. In that case the following phenomena should be taken into account [6,36].

(i) The axial ambipolar electric field pushes the ions (charge qe) of mobility μ_q out of the plasma; the mobility is defined as usual by the formula (5) (ν is the collision frequency of the ions)

$$\mu_q = \frac{qe}{m\nu}. \tag{5}$$

(ii) Ions experience a random thermal motion, which can make them diffuse out of the plasma. This mechanism can induce both a radial transport over a characteristic length a (radius of the chamber) and an axial transport over a characteristic scale L (half-length of the plasma). In this study only parallel confinement times can be estimated since only axial fluxes are measured.

These (axial) transport phenomena lead, respectively, to the following confinement times (units: τ, s; L, cm; n_e, cm^{-3}; Ti, eV; E, V/cm):

$$\tau_q = 7.1\times10^{-20} L q \ln\Lambda \sqrt{A}\frac{n_e Z_{\text{eff}}}{T_i^{3/2}E}, \tag{6}$$

$$\tau_q = 7.1\times10^{-20} L^2 q^2 \ln\Lambda \sqrt{A}\frac{n_e Z_{\text{eff}}}{T_i^{5/2}}, \tag{7}$$

where A is the atomic mass number, n_e the electron density, Z_{eff} the usual effective charge of the plasma,

$$Z_{\text{eff}} = \frac{\sum_q n_q q^2}{n_e},$$

E the electric field, and $\ln\Lambda$ the Coulomb logarithm. Both schemes show that the confinement time increases as the density increases; however, it decreases as the ion temperature increases. The first mechanism leads to a linear dependence of the confinement time on the charge, while the second mechanism leads to a quadratic law. It is interesting to compare experimental values of the confinement times with the theoretical models: as the ion temperature is in the range of 1 eV it is reasonable to expect that the electric field is of the order of 1 V/cm. Taking $\ln\Lambda=15$, $n_e=10^{12}\,cm^{-3}$, $L=3$ cm (half-length of the plasma, i.e., the resonance zone); and $Z_{\text{eff}}=8.5$ (optimization of Ar^{16+}), the following values are obtained:

$$\tau_{9+}=1.5\text{ ms};\quad \tau_{16+}=2.7\text{ ms}$$

for the confinement time using Eq. (6), while the following values are obtained:

$$\tau_{9+}=42\text{ ms};\quad \tau_{16+}=132\text{ ms}$$

with Eq. (7).

Our measurements therefore suggest that the first mechanism [Eq. (6)] is more suited to describe the confinement in an ECR ion source, as it leads both to the correct dependence on charge and also to the correct order of magnitude. In this confinement scheme, however, there is no potential dip as assumed in the derivation of Eq. (4) (potential dip model): the sign of the electric field is such as to expel the ions, not to confine them as in the potential dip model. This raises the important question: is there any potential dip in an ECRIS? Such a potential dip related to ECR heating is well known in fusion devices (ECR heating was only an additional heating and it modified the profile of the electric field), but it has never been clearly measured in an ECRIS, which is a device where ECR heating is the only production process of the plasma, with much cooler and much heavier ions than in fusion devices. In Constance B [10] the ions were much warmer (15 eV) than in our device (the reason why the ions are so hot in Constance B was not explained, however). In ECRIS's it seems that the collisionality of the ions is so high and their temperature so low, that it is not necessary to assume that they are confined by any supplementary mechanism such as electrostatic trapping in a potential dip to account for the very high charge states that can be reached in such devices. The potential dip model is most probably well suited to low-collisional protons such as in fusion devices, but not adapted to the cold collisional heavy ions of ECRIS's. Our measurements then suggest another confinement scheme from the one usually assumed in numerical calculations [37].

VI. CONCLUSION

In this paper we presented a diagnostic for characterization of ECRIS plasmas. The highly charged ions were studied *in situ* in order to improve comprehension of ion confinement mechanisms in these particular plasmas. A high-throughput, high-resolution Bragg spectrometer was designed and built for this purpose. The $K\alpha$ emission spectra of highly charged argon ions are presented for various plasma parameters. The most important result is the strong

correlation between the x-ray spectra and the extracted currents.

As EDFs were determined by analysis of the bremsstrahlung emission, ion densities of Ar^{9+} to Ar^{16+} were estimated. We demonstrated that whatever the ECRIS settings the extracted electrical currents are an image of the densities in the plasma. This experimental result makes it possible to verify some assumptions about the ion confinement mechanism: it appears that the best candidate mechanism for ion transport is the mobility of ions in the ambipolar electric field. This mechanism will therefore be taken into account in the ECRIS simulation codes that are developed in the laboratory [3]. In the future a spatial study of ion densities could be carried out using a new ECRIS fitted with several radial accesses to the plasma.

This study has also shown that ECRIS plasmas are well adapted for very high precision atomic physics measurements. Indeed, ECRIS's are efficient ion traps. The x-ray line emission is intense even for low density ions (10^{-4}–10^{-5} times the electron density) and free of Doppler broadening. Using an improved x-ray spectrometer and a current high-performance ECRIS it is now possible to measure very accurately x-ray wavelengths or line widths of heavy highly charged ions.

ACKNOWLEDGMENTS

The authors wish to thank Dr. P. Platz from CEA/Cadarache and A. Gabriel and F. Dauvergne from EMBL/Grenoble for their help in the spectrometer design. We are grateful for the MCDF calculations provided by Dr. P. Indelicato and F. Parrente. We also acknowledge Dr. G. Melin for many fruitful discussions on ionic confinement processes.

[1] R. Geller, *Electron Cyclotron Resonance Ion Sources and ECR Plasmas* (Institute of Physics, Bristol, 1996).
[2] G. Melin *et al.*, Rev. Sci. Instrum. **61**, 236 (1990).
[3] A. Girard, C. Perret, C. Lécot, F. Bourg, H. Khodja, and G. Melin, in *Proceedings of the 1996 International Conference on Plasma Physics*, edited by H. Sugai and T. Hayashi (Japan Society of Plasma Science, Nagoya, 1997), Vol. 1, p. 462.
[4] C. Barué, M. Lamoureux, P. Briand, A. Girard, and G. Melin, J. Appl. Phys. **76**, 2662 (1994).
[5] G. Melin, F. Bourg, P. Briand, M. Delaunay, G. Gaudart, A. Girard, D. Hitz, J. P. Klein, P. Ludwig, T. K. Nguyen, M. Pontonnier, and Y. Su, Rev. Sci. Instrum. **65**, 1051 (1994).
[6] G. Melin and A. Girard, in *Accelerator-Based Atomic Physics Techniques and Applications*, edited by S. M. Shafroth and J. C. Austin (AIP, Woodbury, NY, 1997).
[7] C. Bernard, Ph.D. thesis, Université Claude Bernard, Lyon, 1996.
[8] I. P. Vinogradov, B. Jettkant, D. Meyer, and K. Wiesemann, J. Phys. D **27**, 1207 (1994).
[9] P. Grübling, D. Küchler, A. Ullrich, T. Werner, and G. Zschornack, Rev. Sci. Instrum. **69**, 1367 (1998).
[10] C. C. Petty, D. L. Goodman, D. L. Smatlak, and D. K. Smith, Phys. Fluids B **3**, 705 (1991).
[11] D. Hitz, P. Ludwig, G. Melin, and M. Pontonnier, Nucl. Instrum. Methods Phys. Res. B **98**, 517 (1995).
[12] B. Jacquot, French Patent No. 83 10862 (1983).
[13] A. G. Drentje, Nucl. Instrum. Methods Phys. Res. B **9**, 526 (1985).
[14] C. P. Bhalla, Phys. Rev. A **8**, 2877 (1973).
[15] H. H. Johann, Z. Phys. **69**, 185 (1931).
[16] A. Gabriel and F. Dauvergne, Rev. Sci. Instrum. **48**, 1303 (1977).
[17] R. J. Dejus, Rev. Sci. Instrum. **67**, 1 (1996).
[18] R. Friedlein, D. Küchler, C. Zippe, and G. Zschornack, Hyperfine Interact. **99**, 225 (1996).
[19] M. Lamoureux and N. Avdonina, Phys. Rev. E **55**, 912 (1997).
[20] L. Kissel, At. Data Nucl. Data Tables **28**, 381 (1983).
[21] K. B. Fournier, M. Cohen, and W. H. Goldstein, Phys. Rev. A **56**, 4715 (1997).
[22] L. B. Golden and D. H. Sampson, J. Phys. B **10**, 2229 (1977).
[23] D. H. Oza, Phys. Rev. A **25**, 2812 (1982).
[24] D. H. Sampson, A. D. Parks, and R. E. Clark, Phys. Rev. A **17**, 1619 (1978).
[25] D. H. Sampson, R. E. Clark, and A. D. Parks, J. Phys. B **12**, 3257 (1979).
[26] J. P. Briand *et al.*, Phys. Rev. A **28**, 1413 (1983).
[27] P. Indelicato and F. Parente (private communication).
[28] M. H. Chen, At. Data Nucl. Data Tables **34**, 301 (1986).
[29] M. H. Chen and B. Crasemann, At. Data Nucl. Data Tables **37**, 419 (1987).
[30] M. H. Chen and B. Crasemann, At. Data Nucl. Data Tables **38**, 381 (1988).
[31] M. H. Chen *et al.*, At. Data Nucl. Data Tables **65**, 289 (1997).
[32] C. Perret, Ph.D. thesis, Université Joseph Fourier, Grenoble, 1998.
[33] C. Perret, A. Girard, H. Khodja, and G. Melin, Phys. Plasmas **6**, 3408 (1999).
[34] V. Pastukhov, Nucl. Fusion **14**, 3 (1974).
[35] T. Rognlien and T. Cutler, Nucl. Fusion **20**, 1003 (1980).
[36] D. R. Waley and W. D. Getty, Phys. Fluids B **2**, 1195 (1990).
[37] H. I. West, Lawrence Livermore National Laboratory Report No. UCRL-53391, 1982 (unpublished).
[38] D. Bolshukhin *et al.*, Rev. Sci. Instrum. **69**, 1197 (1998).
[39] T. Nakagawa, Rev. Sci. Instrum. **69**, 637 (1998).